Orbital molecules in vanadium oxide spinels

Alexander J. Browne and J. Paul Attfield [*]

Centre for Science at Extreme Conditions and School of Chemistry, University of Edinburgh, West Mains Road, Edinburgh EH9 3FD, United Kingdom

X-ray scattering and magnetization measurements have been used to explore the extent of orbital molecule formation in a variety of AV_2O_4 vanadium oxide spinels. Zn doping suppresses the long-range order of trimer-tetramer pairs that occurs in GaV_2O_4, but disordered orbital molecules are found across most of the $Zn_xGa_{1-x}V_2O_4$ series ($0.06 \leqslant x < 0.875$). Orbital molecules are not observed in the ground states of ZnV_2O_4, MgV_2O_4, or LiV_2O_4 but are likely present in $Li_{0.5}Ga_{0.5}V_2O_4$, an analog of the former two materials. The ratio of observed to ideal values of the V-V nearest-neighbor distance has been used to rationalize these observations.

I. INTRODUCTION

The electronic and magnetic states of transition-metal oxides with strongly correlated d electrons can be described in terms of charge, spin, and orbital degrees of freedom [1,2]. These can interact to produce a great variety of electronic ground states, as electron-electron correlations can be static or dynamic and exist over length scales ranging from nearest-neighbor interactions to long-range crystalline periodicity. They are also often highly sensitive to perturbations, even within a given structural family. For example, several AV_2O_4 vanadium oxides crystallize in the normal spinel structure [Fig. 1(a)] but their ground states vary considerably: while heavy-fermion correlations dominate in LiV_2O_4 [3], ZnV_2O_4 is an antiferromagnet [4], and vanadium orbital molecules form in AlV_2O_4 [5]. The extent of the latter ground state has been explored here.

Orbital molecules are covalently bonded clusters of transition-metal cations embedded within an extended lattice [6]. They can form in materials where the d orbitals of neighboring cations interact directly with one another via t_{2g}-t_{2g} overlap through edge- or face-sharing metal oxide octahedra. Accordingly the rutile and spinel structures, in which octahedra form edge-sharing chains in one and three dimensions, respectively, are common hosts. Spinel examples include $MgTi_2O_4$, in which Ti_2^{6+} dimers form along helical chains [7], $CuIr_2S_4$, in which Ir_2^{8+} dimers organize into eight-membered rings [8], and Fe_3O_4, in which Fe_3^{8+} trimerons order below the Verwey transition [9]. A prominent rutile type is VO_2, which undergoes a Peierls-like metal-insulator transition at 340 K that is associated with the formation of V_2^{8+} orbital dimers [10]. Structurally related to VO_2 are the Magnéli phases such as V_4O_7, which also have dimer ground states [11]. In V^{3+} systems the $3d^2$ configuration allows each cation to form two bonds so that V_3^{9+} trimers form in $LiVO_2$ [12], $Na_{0.5}VO_2$ [13], and $BaV_{10}O_{15}$ [14]. Seven-atom, 18-electron vanadium "heptamers" were initially

reported in the charge-ordered ground state of AlV_2O_4 [15], but a subsequent x-ray atomic pair distribution function (PDF) analysis revealed these orbital molecules to be V_3 trimers and V_4 tetramers [5]. They are arranged as disordered V_3-V_4/V_4-V_3 pairs in the low-temperature superstructure of AlV_2O_4 and they persist in a disordered state within the high-temperature cubic spinel state. Similar orbital molecule states were subsequently found in the analog material GaV_2O_4 [16].

The spinel structure is an excellent template for exploring orbital molecule phenomenology as the three-dimensional connectivity of edge-sharing VO_6 octahedra allows for a range of bonding arrangements, and orbital molecule formation also relieves the geometric frustration of ordering interactions over the pyrochlore sublattice of the V sites [Fig. 1(b)]. Previous experimental and theoretical studies of other vanadium oxide spinels, such as ZnV_2O_4 [17] and LiV_2O_4 [18], have suggested that V–V bonding interactions may also play a role in their correlated ground states. These suggestions, coupled with our studies of AlV_2O_4 and GaV_2O_4 mentioned above, motivated the present work. As done for AlV_2O_4 and GaV_2O_4, we have employed x-ray total scattering from polycrystalline samples to search for local structural distortions that result from disordered orbital molecules hidden within the crystallographic average structure. We have also used magnetization measurements and powder-neutron diffraction to explore the magnetic properties of selected materials. A range of spinels have been studied and the Results sections are arranged in order of decreasing V electron count (increasing charge state): solid solutions between $3d^{2.5}$($V^{2.5+}$) GaV_2O_4 and $3d^2$(V^{3+}) ZnV_2O_4; the latter and the other $3d^2$(V^{3+}) spinels MgV_2O_4 and $Li_{0.5}Ga_{0.5}V_2O_4$, a new A-site disordered variant; and $3d^{1.5}$($V^{3.5+}$) LiV_2O_4.

II. EXPERIMENTAL

A. Synthesis

Polycrystalline powder samples of all materials were prepared by high-temperature solid-state reactions as detailed
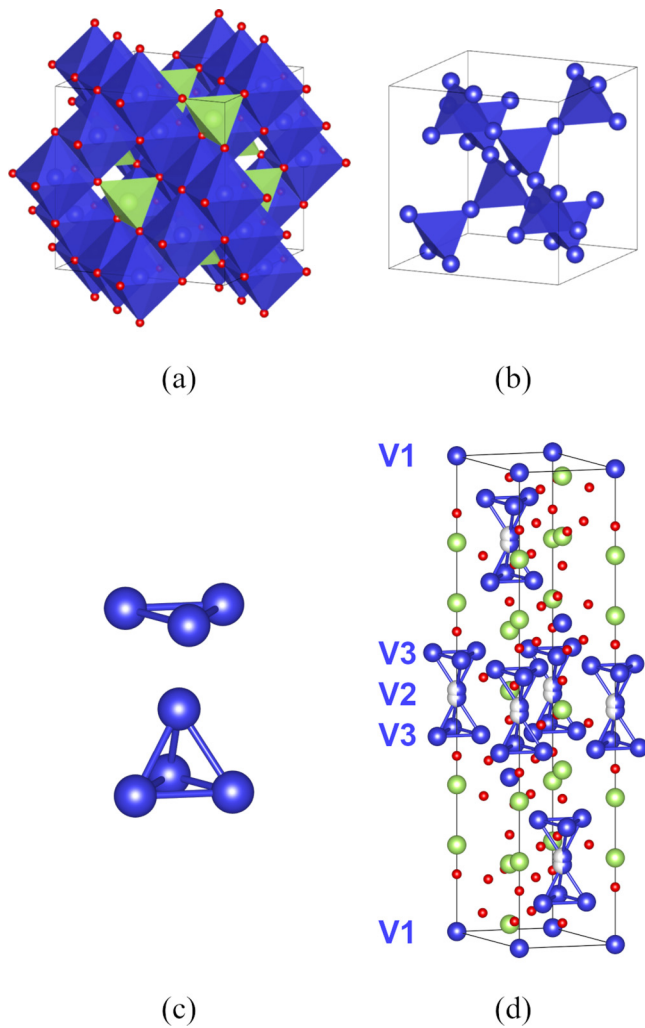
[*]j.p.attfield@ed.ac.uk

FIG. 1. (a) Ideal AV_2O_4 spinels adopt a cubic $Fd\bar{3}m$ crystal structure in which the A-site (green) and vanadium (blue) cations are tetrahedrally and octahedrally coordinated by oxide anions (red), respectively. Each VO_6 octahedron shares edges with six neighbors, such that the vanadium cations themselves form (b) a pyrochlore sublattice of corner-sharing tetrahedra. (c) In AlV_2O_4 and GaV_2O_4, V_3^{9+} trimers and V_4^{8+} tetramers are formed through strong local V–V bonding interactions. In the ground state these order as trimer-tetramer pairs, although the weak interactions between pairs means that each can adopt one of two configurations (V_3-V_4 or V_4-V_3) in (d) the $R\bar{3}m$ average structure. The three vanadium crystallographic sites in this structure are labelled.

below. Powder-x-ray diffraction, using a Bruker D2 Phaser diffractometer equipped with a Cu anode, was used to confirm that reactions had reached completion.

GaV_2O_4, ZnV_2O_4, and $Zn_xGa_{1-x}V_2O_4$ solid solutions were synthesized from ZnO, Ga_2O_3, V, and V_2O_3 powders, the latter prepared in advance by the reduction of V_2O_5 under flowing H_2 at 900 °C, in the stoichiometric ratio appropriate for the composition. These were ground together and pressed into pellets, which were sealed individually in evacuated quartz ampoules prior to heating. This was carried out for 48 h at 1000 °C for phases with $0 \leqslant x < 0.125$, and for 48 h at 900 °C for phases with $0.125 \leqslant x \leqslant 1$.

MgV_2O_4 was synthesized from MgO and V_2O_5. A pellet of the ground powders in the stoichiometric ratio was first heated under flowing H_2, for 2 h at 600 °C and then 12 h at 1080 °C. Subsequently the pellet was ground and pressed again, then heated at 1100 °C for 48 h in an evacuated quartz ampoule.

$Li_{0.5}Ga_{0.5}V_2O_4$ was synthesized by the reaction of $LiGaO_2$ and V_2O_3. The former was prepared by heating Li_2CO_3 (with 5% molar excess) and Ga_2O_3 for 12 h at 900 °C, and the latter by the reduction of V_2O_5. Stoichiometric quantities of these precursors, plus additional Li_2CO_3 to provide a 10% excess of Li, were ground together and transferred to a gold capsule, which was sealed in an evacuated quartz ampoule. This was heated at 850 °C for 72 h, then quenched to room temperature.

To synthesize LiV_2O_4, V_2O_3 was prepared by the reduction of V_2O_5 as above, and Li_3VO_4 was prepared by the reaction of Li_2CO_3 and V_2O_5 (with a 5% molar excess of the former) for 36 h at 800 °C. A pellet consisting of these precursors and V_2O_5 in the stoichiometric ratio was sealed in a gold capsule within an evacuated quartz ampoule, which was heated at 900 °C for 48 h.

B. X-ray total scattering

All x-ray total scattering data were collected at beamline ID22 of the European Synchrotron Radiation Facility, set up with a PerkinElmer XRD1611 2D detector to access high-Q scattering.

Two experiments were conducted to study the $Zn_xGa_{1-x}V_2O_4$ system. In the first, a He cryostat was used for temperature control and data were collected for the phases with $x = 0$ (at temperature steps between 5 and 280 K), $x = 0.125$ (5–280 K), $x = 0.875$ (5–280 K), and $x = 1$ (10–280 K), and also for MgV_2O_4 (10–100 K). In the second, a N_2 cryostream was used and data were collected for all synthesized $Zn_xGa_{1-x}V_2O_4$ phases at both 90 and 300 K. Additional data were collected at steps on warming from 300 to 500 K for $x = 0$, 0.02, and 0.04, and on warming from 90 to 300 K for $x = 0.06$.

Experimental parameters and data processing were kept as consistent as possible between the two experiments. Both used 70-keV radiation, with calibrated wavelengths of 0.177 022 Å for the first and 0.176 938 Å for the second. Each sample was held in a borosilicate capillary of 0.5-mm diameter, and the total scattering pattern of each sample at each temperature step was the average of 201 1-s exposures. Rietveld analysis of these patterns was done using GSAS [19]. PDFGETX3 [20] was used to make background corrections to these patterns, convert them to structure functions $S(Q)$, and transform these to PDFs $G(r)$. These transforms were done for momentum transfers $1.0 \leqslant Q(\text{Å}^{-1}) \leqslant 19.2$ for the first experiment and $0.5 \leqslant Q(\text{Å}^{-1}) \leqslant 20.0$ for the second; the reduced range in the former case was needed to avoid background anomalies from the cryostat that could not be properly corrected for. Fits of structural models to these PDFs were done using PDFGUI [21], for the interatomic distances $1.5 \leqslant r(\text{Å}) \leqslant 12.0$ in all cases, and included simulation of termination ripples.

Total scattering data were collected for LiV_2O_4 in a separate experiment. The sample was loaded into the He cryostat in a 0.7-mm capillary, and data were collected on warming from 5 K to room temperature using 60-keV radiation ($\lambda =$

0.206 547 Å). 201 exposures, each of 1.5 s, were averaged to give the total scattering pattern at each temperature step. Rietveld analysis was done using GSAS; PDFs were generate using PDFGETX3, for $0.5 \leqslant Q(\text{Å}^{-1}) \leqslant 20.2$; and fitting of these including simulation of termination ripples was done using PDFGUI over the range $1.5 \leqslant r(\text{Å}) \leqslant 10.0$.

C. Magnetometry

DC magnetic susceptibility measurements were made for all synthesized samples using a Quantum Design superconducting quantum interference device MPMS-XL. An applied field of 5000 Oe was used for the measurements on GaV_2O_4, ZnV_2O_4, MgV_2O_4, and all $Zn_xGa_{1-x}V_2O_4$ phases, while 1000 Oe was used for $Li_{0.5}Ga_{0.5}V_2O_4$ and LiV_2O_4.

D. Powder-neutron diffraction

Powder-neutron-diffraction data were collected for $Li_{0.5}Ga_{0.5}V_2O_4$ using the HRPD beamline at the ISIS pulsed neutron and muon source. 2.6 g of the sample, held in a slab-geometry vanadium can, was cooled to 4.2 K using a standard orange cryostat; then data were collected at temperature steps on warming to 300 K. GSAS was used to refine structural models against the diffraction patterns collected by the 168° detectors.

III. RESULTS

A. $Zn_xGa_{1-x}V_2O_4$

Previous studies have established that below the charge-ordering transition temperatures $T_{CO} = 700$ and 415 K, respectively [5,16], AlV_2O_4 and GaV_2O_4 adopt an $R\bar{3}m$ spinel superstructure in which pairs of a V_3 trimer and a V_4 tetramer with shortened V-V distances have long-range order [Figs. 1(c) and 1(d)]. Magnetic susceptibility measurements reveal that these orbital molecules are spin singlets, and their bonding follows a simple two-center two-electron scheme that corresponds to the charge-ordering pattern $A_4[V_4^{8+}V_3^{9+}V^{3+}]O_{16}$. The remaining V^{3+} $S = 1$ cation spins freeze or order below a transition at 3.8 K for A = Ga. Above T_{CO}, these materials have the cubic $Fd\bar{3}m$ cell of the normal spinel structure, but x-ray total scattering has shown that V–V bond shortening persists up to at least 1100 K due to the presence of disordered V_3 and V_4 orbital molecules. The robustness of the orbital molecules to temperatures far above T_{CO} suggests that they may also persist upon doping, hence we have investigated long-range and local structural correlations across the $Zn_xGa_{1-x}V_2O_4$ system.

Rietveld fits to the Bragg x-ray-diffraction peaks were used to determine how the lattice symmetry and parameters evolve. Small amounts of Zn doping are found to suppress the $R\bar{3}m$-$Fd\bar{3}m$ charge-ordering transition (Fig. 2). The transition is clearly observed near 400 K for the $x = 0$, 0.02, and 0.04 samples, but no distortion of the cubic crystal structure is seen for $x = 0.06$ down to 90 K. This demonstrates that the long-range order of V_3-V_4 orbital molecule pairs is sensitive to the disorder induced by Zn substitution. More highly doped samples, with x increasing from 0.125 to 0.875 in increments of 0.125, were found to have $Fd\bar{3}m$ spinel average structures
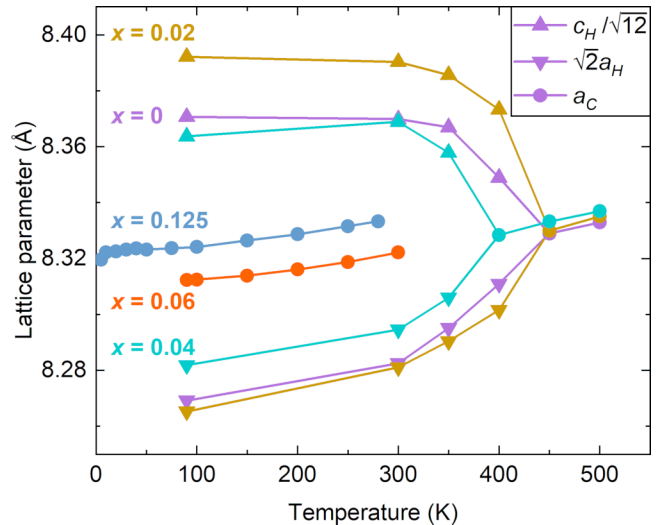

FIG. 2. Lattice parameters of $Zn_xGa_{1-x}V_2O_4$ phases with $x \leqslant 0.125$, from Rietveld refinements of $R\bar{3}m$ (a_H and c_H) and $Fd\bar{3}m$ (a_C) unit cells against x-ray total scattering data. The rapid suppression of the $R\bar{3}m$-$Fd\bar{3}m$ distortion at T_{CO} with increasing x demonstrates that long-range orbital molecule order is highly sensitive to A-site disorder.

at all investigated temperatures. The $x = 1$ material, ZnV_2O_4, has low-temperature orbital- and spin-ordering transitions as described in Sec. III B.

To determine how local structure evolves across the $Zn_xGa_{1-x}V_2O_4$ system we analyzed the x-ray scattering data in two ways, following our previous analyses of AlV_2O_4 [5] and GaV_2O_4 [16]. Rietveld fits to the Bragg diffraction intensities use the $R\bar{3}m$ model in Fig. 1(d) for the rhombohedral phases, where the displacements of the V2 and V3 sites from their ideal spinel positions quantify the degree of orbital molecule formation. For fits to the cubic $Fd\bar{3}m$ phases a split-site model for the V atom in the cubic spinel structure, where 7/8 of the vanadium site occupancy can displace away from the ideal cation position, was used. This displacement quantifies the average degree of orbital molecule formation. Additionally, PDF analysis of the total scattering data, which includes diffuse as well as Bragg contributions, allows changes to the V–V bonding to be assessed on the local scale. Fits to the PDFs were made using an $R3m$ model of ordered V_3-V_4 cluster pairs [5] with the hexagonal lattice parameters a_H and c_H constrained to be metrically cubic when the observed lattice symmetry was $Fd\bar{3}m$. The positions of the V2 and V3 sites that make up the V_3 and V_4 clusters were refined independently, and their displacements from ideal spinel positions again quantify the degree of orbital molecule formation.

The results from Rietveld refinements to 90 K scattering patterns, in Fig. 3(a), show that the cell parameter of the cubic lattice adopted when $x \geqslant 0.06$ increases with x. However, a substantial local V displacement that decreases only slowly up to $x = 0.625$, then more rapidly as x is increased further, is observed in these cubic phases. Part of this displacement is likely due to correlation between the refined displacement and thermal parameters of the V site—-a comparison of the R_w
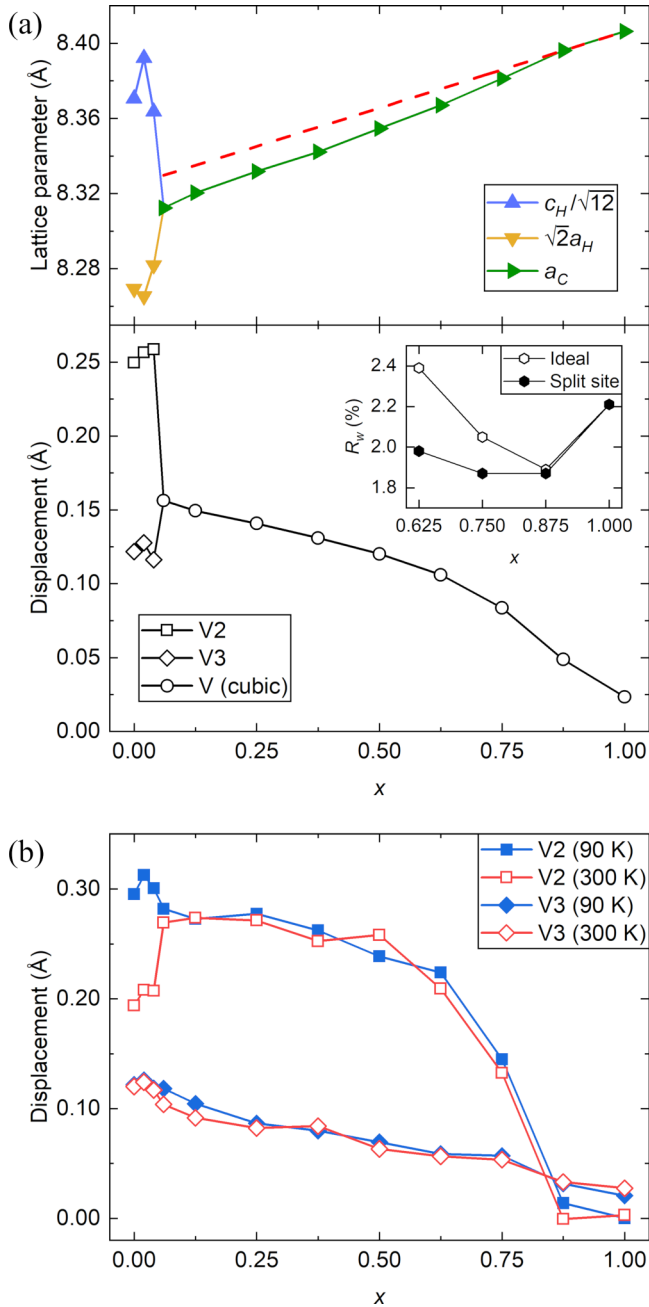
FIG. 3. (a) Average-structure parameters across the $Zn_xGa_{1-x}V_2O_4$ system, from Rietveld fits to 90 K total scattering data. Phases with $x \leqslant 0.04$ adopt $R\bar{3}m$ symmetry, which allows V_3-V_4 cluster pairs to establish long-range order through a displacive distortion of the ideal $Fd\bar{3}m$ lattice. For $x \geqslant 0.06$ there is no periodic distortion, but significant displacement of the vanadium cations from their ideal (zero-displacement) position indicates disorder in the average structure that arises from local symmetry lowering. In the inset, R_w values of Rietveld fits with V fixed at its ideal position or displaced as a split site are shown. (b) Refined displacements of the V2 and V3 crystallographic sites of the $R3m$ structural model when fit to $Zn_xGa_{1-x}V_2O_4$ PDFs. These remain nonzero through the periodic distortion at low x, demonstrating that the orbital molecules persist through this distortion, although the critical-type decrease of the V2-site displacement when approaching $x = 0.875$ evidences their eventual decomposition.

residuals for fits in which V was either held at the ideal site or allowed to refine as a split site, with the thermal parameter refined in both cases [Fig. 3(a), inset], shows that the split-site model offers no significant improvement for $x = 0.875$ and $x = 1$ but does evidence local displacements for $x < 0.875$ samples.

The V-atom displacements from PDF analysis, in Fig. 3(b), are comparable to those determined in the Rietveld refinements. As x increases the displacements determined from the PDF fits vary continuously through the crystallographic distortion that occurs between $x = 0.04$ and 0.06. This implies that the orbital molecules undergo a substitution-induced order-disorder transition equivalent to the temperature-induced one that occurs at T_{CO} in the low-x phases. It is also notable that as x approaches 0.875, the V2-site displacement decreases rapidly to zero with a critical-type behavior. This suggests that a well-defined transition from a state in which disordered orbital molecules are present to one where they are absent takes place at this level of doping. This is corroborated by the variation of the 90 K cubic lattice parameter a_C in Fig. 3(a). A small anomaly in the slope is evident at $x = 0.875$, and extrapolating linearly from the $x = 0.875$ and 1 points shows an excess decrease in a_C below $x = 0.875$ that mirrors the critical-type variation of the V2 displacement in Fig. 3(b). Similar behavior of a_C at 300 K is shown in the Supplemental Material [22]. Hence, the shortening of V-V distances within orbital molecules leads to a slight lattice shrinkage for $x < 0.875$ samples.

Evidence for this transition can also be seen in a comparison of fits of the $R3m$ model that describes local orbital molecules and the $Fd\bar{3}m$ model of the uniform average structure to the PDFs of the $x = 0.125$ and 0.875 samples. Even at 5 K, the fit to the former [Fig. 4(a)] is significantly improved when the local symmetry is lowered, while for the latter [Fig. 4(b)] it is not. Furthermore, for these materials and GaV_2O_4, variable-temperature fits show that there are no significant changes to their local structures between 5 and 300 K [Fig. 4(c)]. The V-V distances that define the orbital molecules in the local structure of GaV_2O_4 are very similar to those obtained from Rietveld fits of the $R\bar{3}m$ average structure. A similar range of local V-V distances is also found in the cubic $x = 0.125$ phase, despite Rietveld analysis only giving the single average value. However, for the $x = 0.875$ phase, PDF fits give short and long V-V distances that differ by little more than their errors, so as noted above there is no convincing evidence for orbital molecule formation in this composition.

Magnetic susceptibility measurements for the $Zn_xGa_{1-x}V_2O_4$ samples are shown in Fig 5(a). They show spin-glass or antiferromagnetic transitions increasing from $T_{spin} = 3.8$ K in pure GaV_2O_4 to 39 K for the antiferromagnetic spin order in ZnV_2O_4. No other transitions are seen up to 300 K, although high-temperature measurements for the $x = 0.04$ sample show an anomaly at 370 K [Fig. 5(a), inset] coinciding with the $R\bar{3}m$-$Fd\bar{3}m$ order-disorder transition at T_{CO}. The susceptibilities of all samples were fit using Eq. (1) between 100 and 300 K; these are provided in Ref. [22]. The three parameters A, C, and θ were fit independently in all cases except ZnV_2O_4, for which
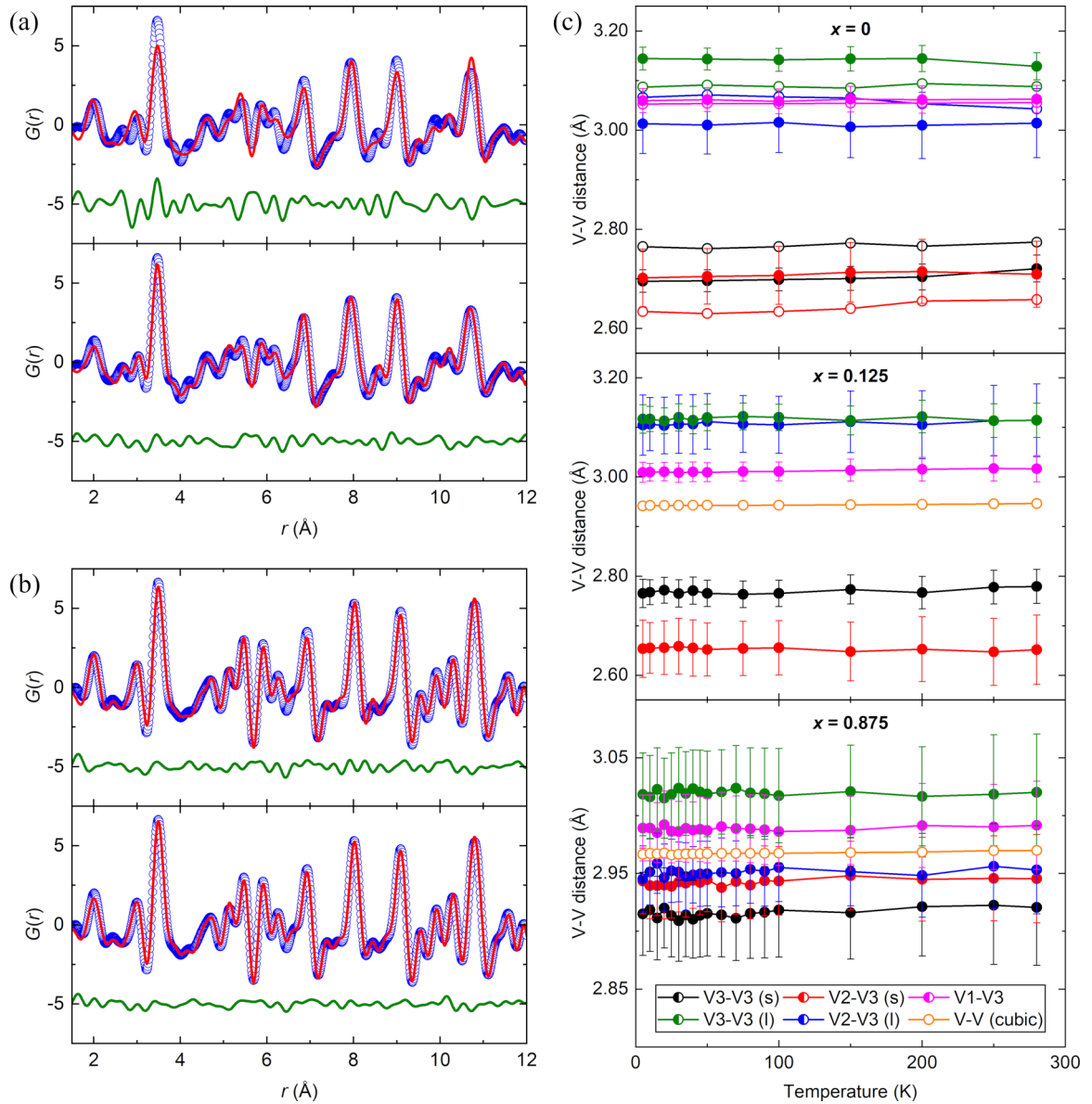
FIG. 4. (a) Fits to the 5 K $x = 0.125$ PDF. Although the average structure has $Fd\bar{3}m$ symmetry a fit of this model (upper, $R_w = 28.9\%$) clearly shows that the local structure deviates from this, and is instead well-described by the $R3m$ model used to describe the local structure of GaV$_2$O$_4$ (lower, $R_w = 15.9\%$). (b) Analogous fits to the 5 K $x = 0.875$ PDF, demonstrating much less local deviation from the cubic average structure ($R_w = 12.4\%$ for $Fd\bar{3}m$, upper; 10.0% for $R3m$, lower). (c) V-V distances in the local (filled symbols) and average (open symbols) structures of the $x = 0$, 0.125, and 0.875 phases, which illustrate the evolution from a ground state of ordered orbital molecules to ones in which they are disordered, and eventually absent, as x is increased.

$A = 2.2 \times 10^{-4}$ emu mol^{-1} was fixed at the literature value [23],

$$\chi = A + \frac{C}{T - \theta}. \qquad (1)$$

As noted previously for GaV$_2$O$_4$ (Ga$_4$[V$_4^{8+}$V$_3^{9+}$V^{3+}]O$_{16}$) [16], A corresponds to the contribution from the V$_4^{8+}$ and V$_3^{9+}$ orbital molecules, which have a large spin gap, while the Curie-Weiss term describes the paramagnetic contribution from the remaining V^{3+} which ideally has $C = 0.25$ emu K mol^{-1} for $S = 1$ spins. The variation of these parameters, and T_{spin}, with x is shown in Fig. 5(b). In the region $0 \leqslant x \leqslant 0.375$, the fitted C decreases from 0.07 to

0.03 emu K mol^{-1}, while θ and T_{spin} show little variation and A increases. The absence of an increase in the paramagnetic contribution confirms that the V ions continue to form spin-singlet orbital molecules on passing from the ordered ($R\bar{3}m$) to disordered ($Fd\bar{3}m$) regimes. This is likely achieved by decreasing the number of V$_4^{8+}$ and increasing the number of V$_3^{9+}$ clusters. It is not straightforward to deduce how the overall V$_4^{8+}$:V$_3^{9+}$: V^{3+} ratio changes with x, but if the proportion of free V^{3+} spins is assumed to be fixed at 1/8 then the overall Zn$_x$Ga$_{1-x}$V$_2$O$_4$ charge balance in this regime is (Zn$_x$Ga$_{1-x}$)$_4$[(V$_4^{8+}$)$_{1-x}$(V$_3^{9+}$)$_{1+4x/3}$V^{3+}]O$_{16}$.

For $x \geqslant 0.5$, the magnitudes of C and θ increase while that of A decreases. This increase of the paramagnetic contribution
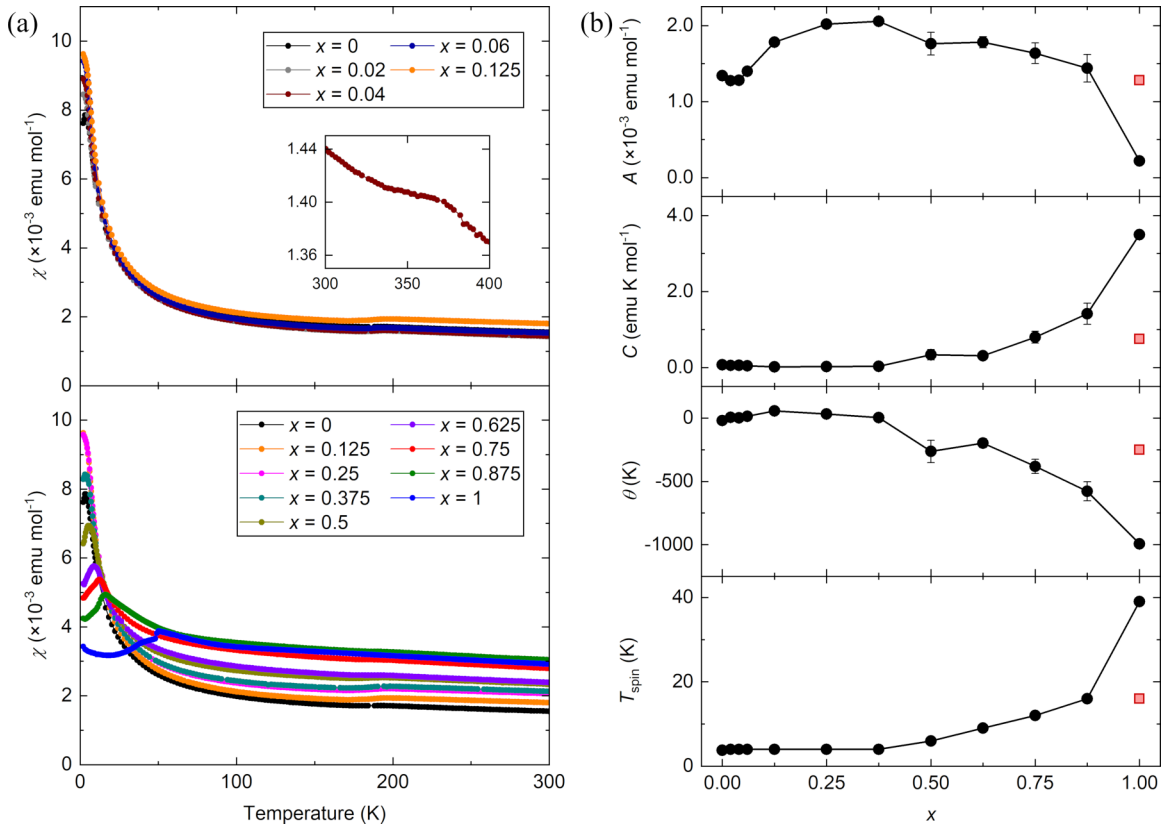
FIG. 5. (a) Magnetic susceptibilities of all synthesized $Zn_xGa_{1-x}V_2O_4$ phases. Their gradual variation with x is consistent with the gradual changes found in the structural analysis. In the inset, the discontinuity seen in the $x = 0.04$ susceptibility at $T_{CO} = 370$ K is shown. Fits of these susceptibilities between 100 and 300 K with Eq. (1) determine (b) the parameters A, C, and θ, which vary as the V–V bonds found in GaV_2O_4 weaken then decompose as x increases. The susceptibilities also all show a magnetic transition at temperature T_{spin}, below which nonbonding V cations establish a spin-glass or antiferromagnetic ordered state. Also shown (red squares) are the parameters obtained from an analogous fit to the susceptibility of $Li_{0.5}Ga_{0.5}V_2O_4$ [Fig. 8(b)], which is isoelectronic with ZnV_2O_4.

to the total susceptibility at the expense of the temperature-independent term is consistent with the breakup of orbital molecules into single paramagnetic ions. This breakup is also evident in the increase of T_{spin} from 4 K at $x = 0.375$ to 16 K at $x = 0.875$ as more paramagnetic cations become available to interact within the spin-glass state. Finally, A, C, θ, and T_{spin} all change dramatically between $x = 0.875$ and 1, which is consistent with complete loss of all orbital molecules and the paramagnetic high-temperature state of ZnV_2O_4 being established. The Curie-Weiss parameters are in agreement with previously reported values $C \approx 3$ emu K^{-1} mol^{-1} and $\theta \approx -1000$ K [24]; these suggest that strong orbital contributions are present. T_{spin} is also markedly larger than for the $x < 1$ spin-glass materials, as it corresponds to the antiferromagnetic transition for ZnV_2O_4 at $T_N = 39$ K.

The magnetism of the $Zn_xGa_{1-x}V_2O_4$ system is thus consistent with the structural behavior deduced from the x-ray scattering data. The orbital molecules in GaV_2O_4 are initially stable as x increases and valence electrons are removed, but gradually decompose when $x \geqslant 0.5$ and are fully lost at around $x = 0.875$. Accordingly, a phase diagram for the $Zn_xGa_{1-x}V_2O_4$ system can be constructed (Fig. 6). The ground state of GaV_2O_4, with its $R\bar{3}m$ lattice of ordered V_3-V_4 orbital molecule pairs, is established below T_{CO} at low x. Long-range order of orbital molecules is rapidly destabilized

by Zn substitution at the spinel A site, but the orbital molecules themselves are remarkably resilient and persist to $x \approx 0.875$. The variable-temperature data demonstrate that when present,
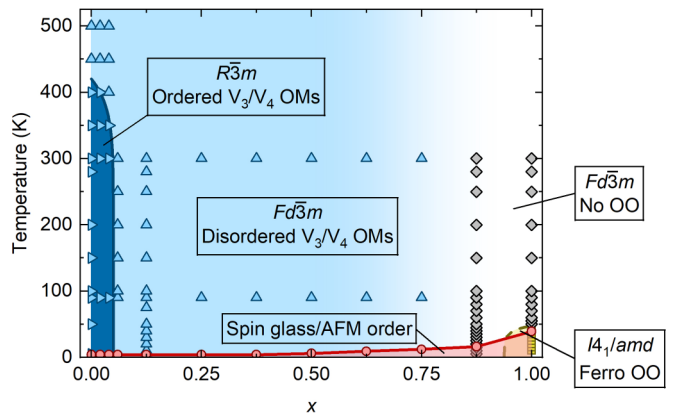

FIG. 6. Phase diagram of the $Zn_xGa_{1-x}V_2O_4$ system. Orbital molecules (OMs) form in most compositions, although they only establish long-range order at low T and when A-site disorder is minimal. V–V bonding weakens as x increases and is fully suppressed near $x = 0.875$. The orbitally ordered (OO) tetragonal ground state of ZnV_2O_4 is established at low T around $x = 1$.

orbital molecules are thermally stable to at least 300 K, and our previous study of $x = 0$ GaV$_2$O$_4$ found that they can be stable up to at least 1100 K. Only for $x \approx 0.875$–1 is an ideal $Fd\bar{3}m$ spinel undistorted by local V–V bonding formed, although the orbitally ordered ground state of ZnV$_2$O$_4$ is established at sufficiently low temperatures. This ground state was not found in any of the other synthesized Zn$_x$Ga$_{1-x}$V$_2$O$_4$ phases, although its destabilization upon Ga substitution can be estimated by comparison to the Li$_x$Zn$_{1-x}$V$_2$O$_4$ system, in which it is suppressed by 10% Li substitution [25].

B. ZnV$_2$O$_4$ and MgV$_2$O$_4$

Previous studies have established that the ground state of ZnV$_2$O$_4$ is established through separate orbital and spin-ordering transitions [4]. Below $T_S = 51$ K the high-temperature $Fd\bar{3}m$ structure undergoes a tetragonal compression that partially lifts the degeneracy of the t_{2g} orbitals by ordering one of the electrons into the d_{xy} orbital but leaving the other shared between degenerate d_{xz} and d_{yz} orbitals. This partial orbital order leads to antiferromagnetic spin order below $T_N = 40$ K with up-down-up-down spin chains in the xy plane but up-up-down-down chains in the xz and yz planes. The same orders are seen in MgV$_2$O$_4$, with $T_S = 62$ K and $T_N = 40$ K [26]. Both materials are Mott insulators, and both antiferro- and ferro-orbital ordering schemes have been proposed [27,28]. However, while some experimental results

have been consistent with the $I4_1/a$ symmetry of the former, others have been consistent with the $I4_1/amd$ symmetry of the latter [29,30]. Powder-neutron diffraction has determined $I4_1/amd$ symmetry for ZnV$_2$O$_4$ [4], while for MgV$_2$O$_4$ super-lattice reflections suggesting $I4_1/a$ symmetry were reported in single-crystal x-ray-diffraction patterns but not in powder x-ray-diffraction patterns [26]. In addition, as the V-V nearest-neighbor distance in these materials is close to the 2.94-Å critical separation for itinerant behavior predicted by Goodenough [31], the possibility of an insulator-metal transition has also been considered [32,33]. Electronic structure calculations have suggested that this occurs through orbital dimerization between the ferromagnetic pairs of spins along xz and yz [17], consistent with the $P4_12_12$ orbital-Peierls dimerized ground state of the spinel MgTi$_2$O$_4$ [34], and chains of alternating short (2.92 Å) and long (3.01 Å) V-V separations have been predicted for such a state in ZnV$_2$O$_4$ [17]. V-V dimers were not identified in previous crystallographic studies of ZnV$_2$O$_4$ and MgV$_2$O$_4$, but neutron spectroscopy has identified phonon anomalies in the latter material that are similar to those from charge fluctuations in other Peierls systems [35].

Magnetic susceptibility measurements on our samples confirm the phase transitions at $T_S = 50$ K and $T_N = 39$ K for ZnV$_2$O$_4$ and $T_S = 57$ K and $T_N = 34$ K for MgV$_2$O$_4$ [22]. Rietveld analysis of x-ray total scattering data confirms that a tetragonal distortion that shortens the c axis of the high-temperature $Fd\bar{3}m$ structure occurs at T_S in both materials,
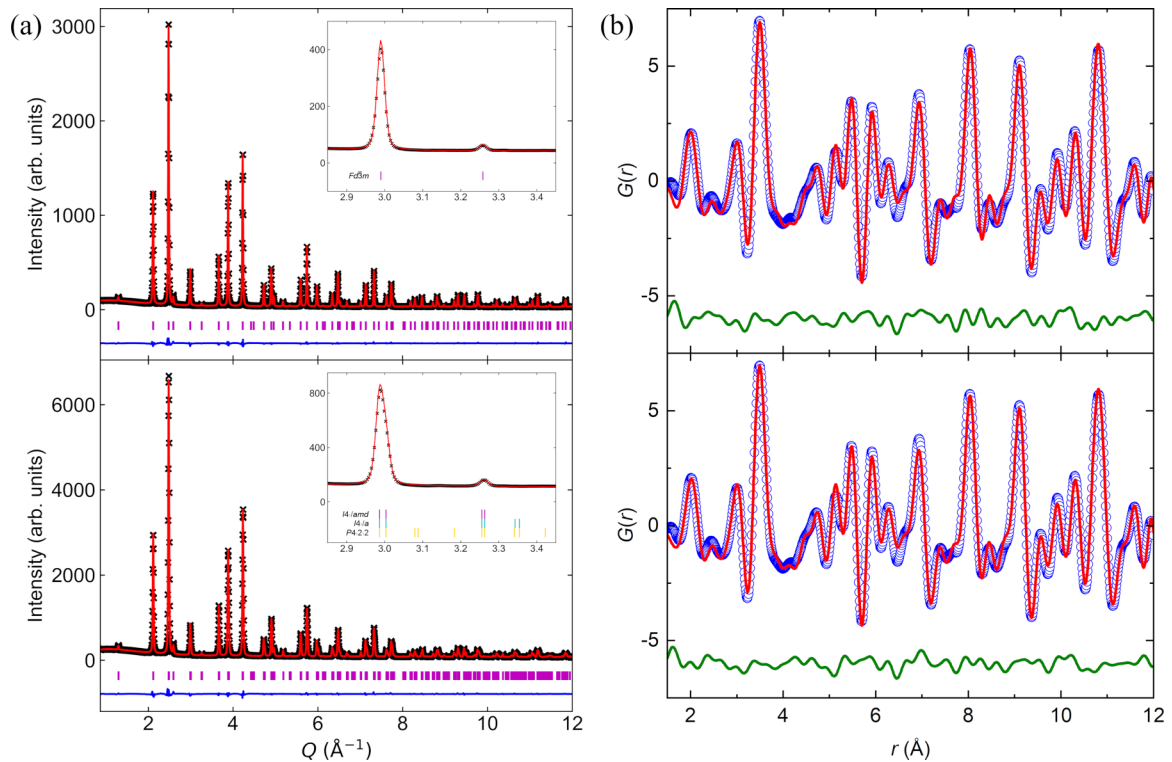

FIG. 7. (a) Rietveld analysis of x-ray total scattering patterns of ZnV$_2$O$_4$. The upper pattern was collected at 100 K and shows an $Fd\bar{3}m$ average structure ($R_w = 2.08\%$) while the lower was collected at 10 K and shows an $I4_1/amd$ average structure ($R_w = 1.96\%$). In the expanded region shown in the insets, the broadening of the cubic 400 ($Q = 2.99$ Å^{-1}) and 331 ($Q = 3.26$ Å^{-1}) reflections by the tetragonal distortion can be seen but the additional reflections of other proposed tetragonal symmetries cannot. (b) Fits to the 10 K x-ray PDF of ZnV$_2$O$_4$. The upper fit is of an $I4_1/amd$ model in which the vanadium site has a fixed position ($R_w = 12.0\%$) and the lower is of a $P4_12_12$ model in which it can displace ($R_w = 10.9\%$).

TABLE I. Refined bond distances obtained from fits of different tetragonal structures to the 10 K PDF of ZnV_2O_4.

Symmetry	$R_w(\%)$	Zn-O (Å)	V-O (Å)	V-V (Å)
$I4_1/amd$	12.0	1.98(5)	1.99(4)	2.966(4)
			2.02(2)	2.978(3)
$I4_1/a$	12.1	1.99(5)	1.99(5)	
			2.02(2)	2.966(5)
			2.02(2)	2.977(3)
$P4_12_12$	10.9	1.95(7)	1.83(5)	
			1.95(8)	2.95(7)
		2.06(5)	2.03(7)	2.97(7)
			2.04(12)	2.98(7)
			2.05(12)	2.98(4)
			2.12(8)	

and the Bragg reflections of the low-temperature phases are both fully indexed by a unit cell of $I4_1/amd$ symmetry [Fig. 7(a) for ZnV_2O_4, Ref. [22] for MgV_2O_4]. This is consistent with the proposed ferro-orbital model for long-range orbital order. The other proposed orderings require a lower tetragonal symmetry ($I4_1/a$ or $P4_12_12$) and the additional Bragg reflections that would arise if one of these was adopted are not seen [Fig. 7(a), insets].

Both $I4_1/amd$ and $I4_1/a$ symmetries do not allow the V atom to move and hence cannot describe V-V dimerization, whereas this is allowed in a $P4_12_12$ symmetry description. To determine whether local vanadium displacements are present in the ground states of ZnV_2O_4 and MgV_2O_4, fits of these three tetragonal structures were made to their 10 K PDFs. For both materials the $I4_1/amd$ and $I4_1/a$ models give very similar fits while that of the $P4_12_12$ model is improved. The $I4_1/amd$ and $P4_12_12$ fits for ZnV_2O_4 are shown in Fig. 7(b) and refined bond distances are given in Table I; the equivalent fits and results for MgV_2O_4 are provided in Ref. [22]. In the $P4_12_12$ fit the AO_4 tetrahedra and VO_6 octahedra are more distorted because this symmetry has more structural degrees of freedom, but the refined atomic positions do not significantly shorten the V-V distances (values for ZnV_2O_4 lie in the range 2.95 to 2.98 Å with errors >0.04 Å).

Hence, this x-ray total scattering study does not evidence V-V orbital dimer formation within the ground states of ZnV_2O_4 and MgV_2O_4. Instead these spinels appear to have a ferro-orbitally ordered ground state that does not involve orbital molecules. However, our study does not rule out spin dimerization as theory has suggested that charge fluctuations in a partially delocalized regime could give rise to the observed antiferromagnetic ground state through spin dimerization of the ferromagnetic V-V pairs with very little bond-length alternation [36]. Neutron total scattering might be useful here to explore local orbital fluctuations through sensitivity to oxygen positions. A previous neutron PDF study used only $I4_1/a$ symmetry in the data analysis [37].

C. $Li_{0.5}Ga_{0.5}V_2O_4$

This previously unreported material has been synthesized to investigate whether A-site cation ordering can be achieved in V^{3+} oxide spinels. In the spinels
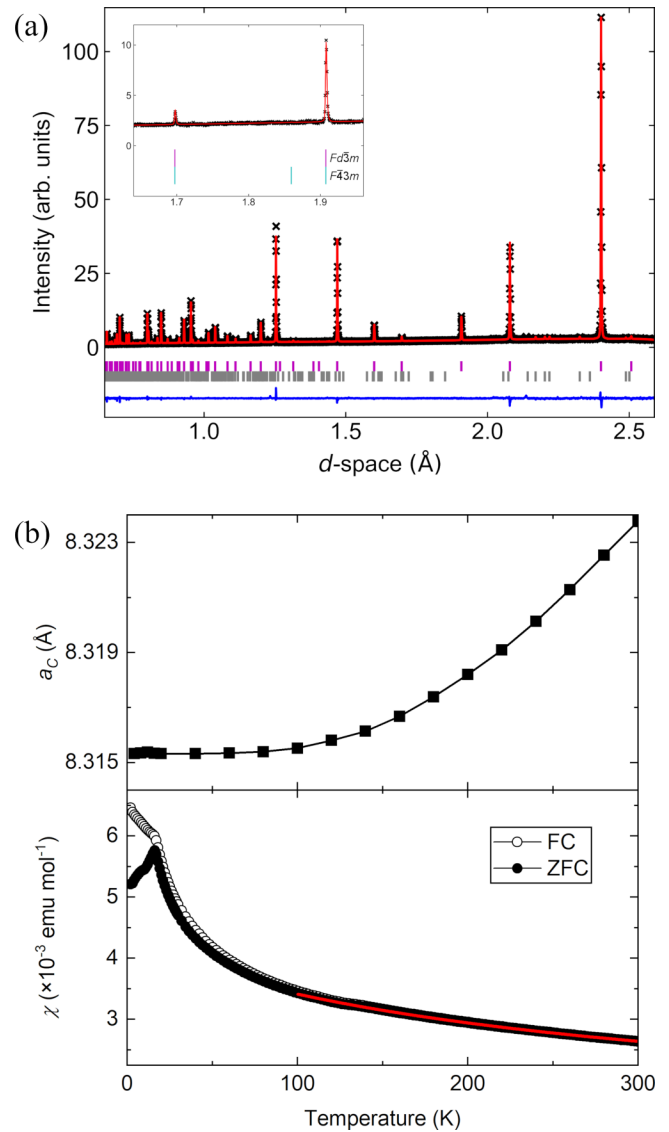

FIG. 8. (a) Rietveld fit to the powder-neutron-diffraction pattern of $Li_{0.5}Ga_{0.5}V_2O_4$ collected at 4.2 K ($R_w = 3.71\%$). Tick marks correspond to the $Fd\bar{3}m$ spinel phase (pink) and a V_2O_3 impurity with 2.2% weight fraction (gray). The additional reflections that would be allowed if the spinel phase adopted $F\bar{4}3m$ symmetry are not observed (expanded region shown in inset). (b) The cubic lattice parameter a_C increases steadily between 4.2 and 300 K. However, its magnetic behavior shows a transition at $T_{spin} = 16$ K, and a fit of Eq. (1) between 100 and 300 K reveals similarity to the $Zn_xGa_{1-x}V_2O_4$ phases with disordered orbital molecule ground states [Fig. 5(b)].

$Li_{0.5}A'_{0.5}Cr_2O_4 (A' = Ga^{3+}, In^{3+})$, a rocksalt-ordered distribution of the A-site cations lowers the cubic symmetry to $F\bar{4}3m$. This allows the Cr^{3+} cations to displace, and they form a "breathing" pyrochlore lattice of alternating small and large Cr_4 tetrahedra [38]. The small Cr_4 tetrahedra are not orbital molecules but a breathing pyrochlore lattice clearly provides a structural template on which orbital molecules could form.

Powder-neutron diffraction reveals that $Li_{0.5}Ga_{0.5}V_2O_4$ has the $Fd\bar{3}m$ cubic spinel structure down to 4.2 K [Fig. 8(a)]. The additional reflections that would arise if this material adopted the $F\bar{4}3m$ symmetry of $Li_{0.5}Ga_{0.5}Cr_2O_4$ are not seen,

despite the high neutron-scattering contrast between Li and Ga, demonstrating that the A-site cations in the vanadium analog have a disordered distribution. The refined A-site occupancy ratio is 0.470(2) Li to 0.530(2) Ga, showing that the sample is slightly Li deficient. Furthermore, the cubic lattice parameter a_C shows a normal thermal expansion behavior between 4.2 and 300 K with no evidence for any structural phase transitions [Fig. 8(b)]. The absence of a tetragonal distortion, or any magnetic diffraction peaks, down to 4.2 K indicates that $Li_{0.5}Ga_{0.5}V_2O_4$ does not have the ordered ground state of isoelectronic ZnV_2O_4 and MgV_2O_4, presumably as long-range orbital- and spin order is suppressed by the A-site cation disorder present in this material.

However, magnetic susceptibility measurements [Fig. 8(b)] reveal a transition at 16 K, and a fit of Eq. (1) to the susceptibility between 100 and 300 K, as was done for $Zn_xGa_{1-x}V_2O_4$ in Sec. III A, gives $C = 0.75(2)\,emu\,K\,mol^{-1}$, $\theta = -251(7)\,K$, and $A = 1.28(3) \times 10^{-3}\,emu\,mol^{-1}$. These values are plotted in Fig. 5(b) for comparison with those of the $Zn_xGa_{1-x}V_2O_4$ phases. Although $Li_{0.5}Ga_{0.5}V_2O_4$ has the same d-electron count as ZnV_2O_4 its magnetic parameters are very different, instead being comparable to values for the $Zn_xGa_{1-x}V_2O_4$ phases with $x = 0.75$ and 0.875. This suggests that disordered orbital molecules are also present in $Li_{0.5}Ga_{0.5}V_2O_4$, although x-ray total scattering data have not been collected to confirm this. Formation of orbital molecules in $Li_{0.5}Ga_{0.5}V_2O_4$, but not in the V^{3+} analogs ZnV_2O_4 or MgV_2O_4, may reflect the smaller lattice parameter of the former material, $a_c = 8.32\,Å$, compared to $a_c = 8.41$ and $8.42\,Å$ for the latter. Li/Ga disorder within the lattice will also create local variations in V-V distances that may help to stabilize orbital molecules.

In summary, although the material $Li_{0.5}Ga_{0.5}V_2O_4$ is isoelectronic to the V^{3+} spinels ZnV_2O_4 and MgV_2O_4, it does not display the same low-temperature orbital- and spin-ordering transitions. Instead, the similarity of its magnetic parameters to those of $Zn_xGa_{1-x}V_2O_4$ phases within the disordered orbital molecule regime suggests that this is the likely ground state of $Li_{0.5}Ga_{0.5}V_2O_4$.

D. LiV_2O_4

At high temperatures LiV_2O_4 is a bad metal with localized-moment magnetism due to strong electron correlations. Below 28 K, these correlations greatly enhance the effective mass of the d electrons such that a heavy-fermion state is formed [3]. This transition is most evident in the corresponding increase of the electronic heat capacity but has also been identified in measurements of other physical properties [39] and of the electronic structure [40,41]. However, the mechanism by which the mass enhancement occurs remains unclear. It is certainly different from the Kondo mechanism that operates in f-electron heavy-fermion systems such as $CeAl_3$; for example, Kondo interactions result in increased resistivity but that of LiV_2O_4 decreases with the mass enhancement [39]. The mass enhancement in LiV_2O_4 is also not accompanied by a long-range distortion of the cubic $Fd\bar{3}m$ crystal structure [42], so geometric frustration of any putative long-range spin, charge, or orbital ordering over the pyrochlore lattice is not relieved and neither magnetic ordering nor spin-glass freezing
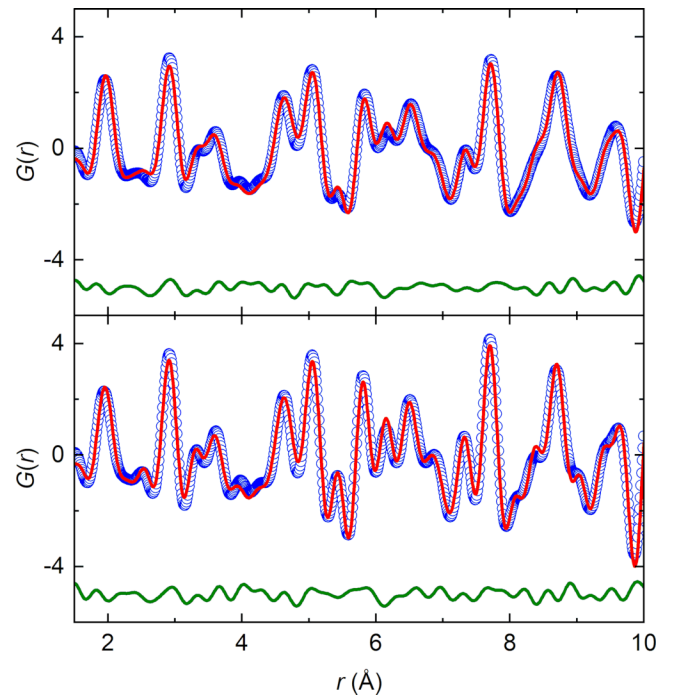

FIG. 9. The PDFs of LiV_2O_4 at 290 K (upper) and 5 K (lower). Both are well fit by an $Fd\bar{3}m$ model consistent with the average structure adopted over this temperature range ($R_w = 11.6$ and 12.3%, respectively).

occurs above 2 K [3]. However, short-range antiferromagnetic fluctuations have been identified [43,44], and neutron scattering has shown that these interactions occur along the V-V chains of the pyrochlore lattice with a partial delocalization of spins that is sufficient for direct cation-cation interactions to occur [18]. Theoretical work incorporating orbital interactions has also suggested that the ground state of LiV_2O_4 can be represented by simple molecular orbitals on V_4 tetrahedra, that the dominant interactions are exchange processes between neighboring tetrahedra, and that the overall properties are determined by local spin and orbital degrees of freedom [45]. These results suggest that V–V bondlike interactions may be significant, and while the lack of a crystallographic distortion rules out an ordered orbital molecule state, the short-range fluctuations involved in the mass enhancement could be related to disordered orbital molecules.

X-ray total scattering data were collected for LiV_2O_4 between 5 and 290 K. Rietveld analysis of these data confirms that the unit cell has cubic $Fd\bar{3}m$ symmetry over this temperature range [22]. Subsequently, structural models were fit to the PDFs of LiV_2O_4 generated from the total scattering data. As would be expected, the 290 K PDF is well fit by an $Fd\bar{3}m$ structural model consistent with the crystallographic unit cell, with a V-V nearest-neighbor distance of 2.915(1) Å ($R_w = 11.6\%$). The 5 K PDF is also fit well by this model, with a V-V nearest-neighbor distance of 2.908(1) Å ($R_w = 12.3\%$) [Fig. 9]. As $Fd\bar{3}m$ symmetry constrains all V-V nearest-neighbor distances to be equal, lower-symmetry models were also fit to the 5 K PDF to try and identify subtle distortions. A cubic $F\bar{4}3m$ structure like that of $Li_{0.5}Ga_{0.5}Cr_2O_4$, in which the vanadium cations could form a breathing pyrochlore lattice, gives distances of 2.908(99) Å and 2.909(99) Å ($R_w =$

12.2%), while a rhombohedral distortion to a simple $R3m$ cell gives distances of 2.90(41) Å, 2.90(45) Å, 2.91(45) Å, and 2.92(41) Å ($R_w = 12.1\%$). The similar values of V-V distances, with very large errors due to refinement instabilities, demonstrate that there are no detectable local structural distortions present within LiV_2O_4 down to 5 K.

As a further check to these, split-site Rietveld refinements that allow the vanadium to displace away from its ideal position were performed. As shown previously for the $Zn_xGa_{1-x}V_2O_4$ system, such refinements allow quantification of any orbital molecule disorder in the average structure, but no significant split-site displacement was found for LiV_2O_4 down to 5 K. We therefore conclude that the electronic fluctuations thought to be responsible for the heavy-fermion mass enhancement in this material at low temperatures are not coupled to a structural distortion on any length scale down to that of V-V nearest neighbors.

IV. DISCUSSION

The above results and those of many previous studies have revealed a wide variety of electronic ground states in the family of AV_2O_4 spinels. The present study, focusing on the formation of orbital molecules, has shown that disordered orbital molecules are present within apparently undistorted cubic spinel materials across most of the $Zn_xGa_{1-x}V_2O_4$ series ($0.06 \leqslant x < 0.875$) and probably also in $Li_{0.5}Ga_{0.5}V_2O_4$. Such local distortions that follow well-defined bonding rules may give rise to correlated disorders [46], other examples of which are the "orbital ice" ground state of Mo_2^{8+} dimers in $Y_2Mo_2O_7$ [47] and the local trimeron distortions that persist in Fe_3O_4 above the Verwey transition [48]. However, there is no structural evidence for local orbital molecule formation from our x-ray total scattering studies of ZnV_2O_4, MgV_2O_4, or LiV_2O_4.

The extent and degree of order of orbital molecules in AV_2O_4 systems can be rationalized through the V d-electron count (charge state) and the V-V nearest-neighbor separation d, which is a crucial parameter in controlling V–V bond formation. We represent the latter through the ratio d/d_{ideal}. In a cubic AV_2O_4 spinel where VO_6 octahedra share edges to form chains in the [110] and equivalent directions, the observed V-V nearest-neighbor separation is given by $d = \sqrt{2}a_C/4$, and an ideal value is given by $d_{ideal} = \sqrt{2}d(V^{m+}-O)$, where the $d(V^{m+}-O)$ is the sum of the ionic radius of the V cation in the appropriate charge state and that of O^{2-}. Hence, we have calculated $d/d_{ideal} = a_C/[4d(V^{m+}-O)]$ using 300 K lattice parameters, and this is plotted against n, the average number of d electrons per V cation, in Fig. 10. This plot nicely stratifies all the materials in this study into different orbital molecule regions. Materials with relatively short V-V separations—AlV_2O_4, GaV_2O_4, and lightly doped $Zn_xGa_{1-x}V_2O_4$—for which $d/d_{ideal} < 0.994$ form ordered orbital molecule arrays within a periodic superstructure. In the intermediate $0.994 < d/d_{ideal} < 1.033$ range, V-V separations are short enough for orbital molecules to form but their local distortions are not sufficient to induce a cooperative order and associated structural transition, hence they remain disordered in the cubic spinel lattice to lowest temperature. Relatively large V-V separations with $d/d_{ideal} > 1.033$

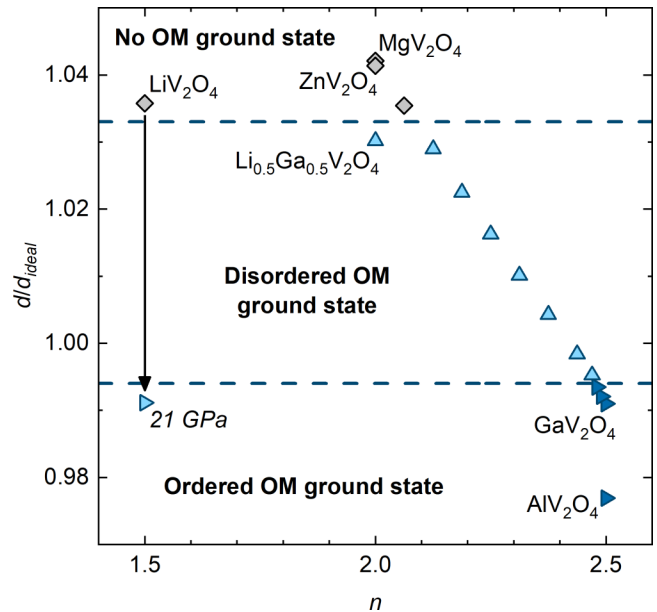FIG. 10. Phase diagram incorporating all AV_2O_4 spinels in this study. d/d_{ideal} is the ratio of observed to ideal values of the V-V nearest-neighbor distance as defined in the text, and n is the average number of d electrons per V cation. The shift in d/d_{ideal} for LiV_2O_4 upon compression to 21 GPa, where V–V bond shortening and a low-temperature lattice distortion have been reported [50], is also shown.

prevent the formation of orbital molecules and this allows other ground states, such as the probable ferro-orbital order in ZnV_2O_4 and MgV_2O_4 and the heavy-fermion itinerant behavior of LiV_2O_4, to emerge. Incipient orbital molecule formation may account for the mass enhancement observed in LiV_2O_4. Pressure-induced changes of structure and properties indicative of V–V bond formation have been reported for the latter material [49,50], and as shown in Fig. 10 it is likely that pressure reduces d/d_{ideal} sufficiently to bring LiV_2O_4 far into the regime of formation and possible order of orbital molecules.

Pressure effects in various $A^{2+}V_2O_4$ spinels have previously been explored as the V-V nearest-neighbor distance is close to the predicted critical value for electron delocalization, so subtle structural perturbations can induce a significant behavioral response [51]. It has been suggested that a transition from the ambient-pressure insulating states to high-pressure metallic ones occur via an intermediate state in which the valence electrons are partially delocalized to form V–V bonds [32]. Pressure-induced structural changes have been observed in ZnV_2O_4, but their relationship to any V–V bonding has not yet been established [33]. The analogous material CdV_2O_4 may even have an orbital molecule ground state at ambient pressure [52], as its ferroelectric behavior has been attributed to variations of V–O bond distances caused by V-V dimerization, but structural confirmation of this has not been reported. However, pressure effects may be complex as pressure also tends to favor delocalized band states over localized orbital molecules. Orbital dimerization is weakened in $MgTi_2O_4$ but strengthened in $CuIr_2O_4$ as pressure is applied [53].

[1] C. N. R. Rao, Annu. Rev. Phys. Chem. **40**, 291 (1989).

[2] Y. Tokura and N. Nagaosa, Science **288**, 462 (2000).

[3] S. Kondo, D. C. Johnston, C. A. Swenson, F. Borsa, A. V. Mahajan, L. L. Miller, T. Gu, A. I. Goldman, M. B. Maple, and D. A. Gajewski *et al.*, Phys. Rev. Lett. **78**, 3729 (1997).

[4] M. Reehuis, A. Krimmel, N. Buttgen, A. Loidl, and A. Prokofiev, Eur. Phys. J. B: Condens. Matter **35**, 311 (2003).

[5] A. J. Browne, S. A. J. Kimber, and J. P. Attfield, Phys. Rev. Mater. **1**, 052003(R) (2017).

[6] J. P. Attfield, APL Mater. **3**, 041510 (2015).

[7] M. Schmidt, W. Ratcliff, P. G. Radaelli, K. Refson, N. M. Harrison, and S. W. Cheong, Phys. Rev. Lett. **92**, 056402 (2004).

[8] P. G. Radaelli, Y. Horibe, M. J. Gutmann, H. Ishibashi, C. H. Chen, R. M. Ibberson, Y. Koyama, Y.-S. Hor, V. Kiryukhin, and S.-W. Cheong, Nature (London) **416**, 155 (2002).

[9] M. S. Senn, J. P. Wright, and J. P. Attfield, Nature (London) **481**, 173 (2012).

[10] J. B. Goodenough, J. Solid State Chem. **3**, 490 (1971).

[11] A. S. Botana, V. Pardo, D. Baldomir, A. V. Ushakov, and D. I. Khomskii, Phys. Rev. B **84**, 115138 (2011).

[12] T. Jin-no, Y. Shimizu, M. Itoh, S. Niitaka, and H. Takagi, Phys. Rev. B **87**, 075135 (2013).

[13] M. Guignard, C. Didier, J. Darriet, P. Bordet, E. Elkaïm, and C. Delmas, Nat. Mater. **12**, 74 (2013).

[14] T. Kajita, T. Kanzaki, T. Suzuki, J. E. Kim, K. Kato, M. Takata, and T. Katsufuji, Phys. Rev. B **81**, 060405(R) (2010).

[15] Y. Horibe, M. Shingu, K. Kurushima, H. Ishibashi, N. Ikeda, K. Kato, Y. Motome, N. Furukawa, S. Mori, and T. Katsufuji, Phys. Rev. Lett. **96**, 086406 (2006).

[16] A. J. Browne, C. Lithgow, S. A. J. Kimber, and J. P. Attfield, Inorg. Chem. **57**, 2815 (2018).

[17] V. Pardo, S. Blanco-Canosa, F. Rivadulla, D. I. Khomskii, D. Baldomir, H. Wu, and J. Rivas, Phys. Rev. Lett. **101**, 256403 (2008).

[18] K. Tomiyasu, K. Iwasa, H. Ueda, S. Niitaka, H. Takagi, S. Ohira-Kawamura, T. Kikuchi, Y. Inamura, K. Nakajima, and K. Yamada, Phys. Rev. Lett. **113**, 236402 (2014).

[19] A. C. Larson and R. B. Von Dreele, Los Alamos National Laboratory Report LAUR 86-748, 2004.

[20] P. Juhás, T. Davis, C. L. Farrow, and S. J. L Billinge, J. Appl. Crystallogr. **46**, 560 (2013).

[21] C. L. Farrow, P. Juhas, J. W. Liu, D. Bryndin, E. S. Božin, J. Bloch, Th. Proffen, and S. J. L. Billinge, J. Phys.: Condens. Matter **19**, 335219 (2007).

[22] See Supplemental Material at http://link.aps.org/supplemental/10.1103/PhysRevB.101.024112 for individual plots and fitting parameters for $Zn_xGa_{1-x}V_2O_4$ magnetic susceptibilities, structural and magnetic data for ZnV_2O_4 and MgV_2O_4, results of x-ray total scattering analysis of MgV_2O_4, and structural and magnetic data for LiV_2O_4.

[23] N. Nishiguchi and M. Onoda, J. Phys.: Condens. Matter **14**, L551 (2002).

[24] H. Mamiya and M. Onoda, Solid State Commun. **95**, 217 (1995).

[25] Y. Ueda, N. Fujiwara, and H. Yasuoka, J. Phys. Soc. Jpn. **66**, 778 (1997).

[26] S. Niitaka, H. Ohsumi, K. Sugimoto, S. Lee, Y. Oshima, K. Kato, D. Hashizume, T. Arima, M. Takata, and H. Takagi, Phys. Rev. Lett. **111**, 267201 (2013).

[27] H. Tsunetsugu and Y. Motome, Phys. Rev. B **68**, 060405(R) (2003).

[28] O. Tchernyshyov, Phys. Rev. Lett. **93**, 157206 (2004).

[29] S.-H. Lee *et al.*, Phys. Rev. Lett. **93**, 156407 (2004).

[30] S. Jung, J. Noh, J. Kim, C. L. Zhang, S. W. Cheong, and E. J. Choi, J. Phys.: Condens. Matter **20**, 175205 (2008).

[31] J. B. Goodenough, *Magnetism and the Chemical Bond* (Wiley-Interscience, New York, 1963).

[32] S. Blanco-Canosa, F. Rivadulla, V. Pardo, D. Baldomir, J. S. Zhou, M. García-Hernández, M. A. López-Quintela, J. Rivas, and J. B. Goodenough, Phys. Rev. Lett. **99**, 187201 (2007).

[33] C. Kuntscher, K. Rabia, M. K. Forthaus, M. M. Abd-Elmeguid, F. Rivadulla, Y. Kato, and C. D. Batista, Phys. Rev. B **86**, 020405(R) (2012).

[34] D. I. Khomskii and T. Mizokawa, Phys. Rev. Lett. **94**, 156402 (2005).

[35] T. Weber, B. Roessli, C. Stock, T. Keller, K. Schmalzl, F. Bourdarot, R. Georgii, R. A. Ewings, R. S. Perry, and P. Böni, Phys. Rev. B **96**, 184301 (2017).

[36] Y. Kato, G. W. Chern, K. A. Al-Hassanieh, N. B. Perkins, and C. D. Batista, Phys. Rev. Lett. **108**, 247215 (2012).

[37] Z. Zhang, D. Louca, A. Visinoiu, S.-H. Lee, J. D. Thompson, T. Proffen, A. Llobet, Y. Qiu, S. Park, and Y. Ueda, Phys. Rev. B **74**, 014108 (2006).

[38] Y. Okamoto, G. J. Nilsen, J. P. Attfield, and Z. Hiroi, Phys. Rev. Lett. **110**, 097203 (2013).

[39] C. Urano, M. Nohara, S. Kondo, F. Sakai, H. Takagi, T. Shiraki, and T. Okubo, Phys. Rev. Lett. **85**, 1052 (2000).

[40] A. Shimoyamada *et al.*, Phys. Rev. Lett. **96**, 026403 (2006).

[41] P. E. Jönsson, K. Takenaka, S. Niitaka, T. Sasagawa, S. Sugai, and H. Takagi, Phys. Rev. Lett. **99**, 167402 (2007).

[42] O. Chmaissem, J. D. Jorgensen, S. Kondo, and D. C. Johnston, Phys. Rev. Lett. **79**, 4866 (1997).

[43] S.-H. Lee, Y. Qiu, C. Broholm, Y. Ueda, and J. J. Rush, Phys. Rev. Lett. **86**, 5554 (2001).

[44] Y. Shimizu, H. Takeda, M. Tanaka, M. Itoh, S. Niitaka, and H. Takagi, Nat. Commun. **3**, 981 (2012).

[45] K. Hattori and H. Tsunetsugu, Phys. Rev. B **79**, 035115 (2009).

[46] D. A. Keen and A. L. Goodwin, Nature (London) **521**, 303 (2015).

[47] P. M. M. Thygesen, J. A. M. Paddison, R. Zhang, K. A. Beyer, K. W. Chapman, H. Y. Playford, M. G. Tucker, D. A. Keen,

M. A. Hayward, and A. L. Goodwin, Phys. Rev. Lett. **118**, 067201 (2017).

[48] G. Perversi, E. Pachoud, J. Cumby, J. M. Hudspeth, J. P. Wright, S. A. J. Kimber, and J. P. Attfield, Nat. Commun. **10**, 2857 (2019).

[49] H. Takeda, Y. Kato, M. Yoshimura, Y. Shimizu, M. Itoh, S. Niitaka, and H. Takagi, Phys. Rev. B **92**, 045103 (2015).

[50] A. J. Browne, E. J. Pace, G. Garbarino, and J. P. Attfield, Phys. Rev. Materials **4**, 015002 (2020).

[51] A. Kismarahardja, J. S. Brooks, A. Kiswandhi, K. Matsubayashi, R. Yamanaka, Y. Uwatoko, J. Whalen, T. Siegrist, and H. D. Zhou, Phys. Rev. Lett. **106**, 056602 (2011).

[52] G. Giovannetti *et al.*, Phys. Rev. B **83**, 060402(R) (2011).

[53] L. Ma, H. Han, W. Liu, K. Yang, Y. Zhu, C. Zhang, L. Pi, D. Liu, L. Zhang, and Y. Zhang, Dalton Trans. **46**, 6708 (2017).